Sensitivity study of mirror energy differences in positive parity bands of $T = \frac{3}{2}$ $A = 45$ nuclei

W. Satuła [1], M. A. Bentley [2], A. Jalili [1], and S. Uthayakumaar [2,3]

[1] *Institute of Theoretical Physics, Faculty of Physics, University of Warsaw, ul. Pasteura 5, PL-02-093 Warsaw, Poland*

[2] *School of Physics, Engineering and Technology, University of York, Heslington, York YO10 5DD, United Kingdom*

[3] *Facility for Rare Isotope Beams, Michigan State University, East Lansing, Michigan 48824, USA*

(Received 7 August 2023; accepted 5 October 2023; published 20 October 2023)

Symmetry-conserving density-functional theory (DFT) based no-core-configuration-interaction framework (DFT-NCCI) is an excellent tool for precision calculation of diverse (pseudo-)observables related to isospin symmetry breaking from elusive isospin impurities through isospin corrections to superallowed beta decays to mirror- and triplet-displacement energies and mirror energy differences (MED) along rotational bands. In our recent work [Phys. Rev. C **106**, 024327 (2022)] we performed axial DFT-NCCI calculations and failed to reproduce a sign of MED in positive-parity ($\pi = +$) bands of ^{45}Sc / ^{45}Cr, $T = 3/2$ mirror pair what casts a shadow on credibility of the model. In this work we aim to perform a thorough analysis of this case with the focus on sensitivity of our predictions with respect to (*i*) low-energy constants (LECs) of our effective contact charge symmetry breaking force and (*ii*) nuclear shape. We demonstrate, among other things, that inclusion of triaxial $\pi = +$ ground state—which is actually the global $\pi = +$ minimum in our unconstrained mean-field calculation—in the DFT-NCCI calculations instead of the axial one used before leads to MED which are consistent with experimental data concerning both their sign as well as magnitude without any need for fine-tuning of the model's LECs.

DOI: 10.1103/PhysRevC.108.044315

I. INTRODUCTION

The origin of isospin symmetry-breaking (ISB) depends on resolution of the underlying theory. At the fundamental level of QCD and/or QED, where the degrees of freedom or, equivalently, the primary building blocks are quarks and gluons, the ISB originates from different masses (strong component) and charges (electromagnetic component) of constituent *up* and *down* quarks. This relatively simple and transparent picture complicates quite radically when quarks and gluons are replaced by point-like nucleons interacting via intermediate mesons. The effective field theories or high-precision meson-exchange potentials contain several sources of ISB which are intertwined. They include, to name a few, nucleon mass splitting, one- and two-boson exchange terms (2π exchange with the intermediate Δ, $\pi\rho$, $\rho\omega$), pion mass splitting, or $\pi\gamma$ exchange. All these terms, following the work of Henley and Miller [1], can be grouped into three distinct classes: class II [isotensor or charge-independence-breaking (CIB)], class III [isovector or charge symmetry breaking (CSB)], and class IV forces. The parameters of high-precision potentials are fit directly to phase shifts (and selected two- and three-body data) and are used subsequently to compute finite nuclei using advanced many-body techniques which do not break manifestly fundamental symmetries. Such methodology is commonly known as an *ab initio* approach to nuclear structure.

Further reduction of degrees of freedom to densities and currents generated by point-like nucleons brings us to the level of approximation commonly known as density-functional theory (DFT). The primary object of interest here is an energy density functional (EDF). In nuclear physics one often explores formal similarity between the Hartree-Fock and Kohn-Sham schemes building the nuclear EDF by means of Hartree-Fock(-Bogolyubov) technology with effective phenomenological EDF generators like the hereafter explored Skyrme interaction, which leads to local DFT. Such formalism, called single-reference DFT (SR-DFT) is a method of choice to compute globally bulk nuclear observables like binding energies, radii, quadrupole moments, or rotational inertia parameters.

The inherent feature of nuclear SR-DFT is a mechanism of spontaneous symmetry breaking (SSB). It is in fact a key to its success in computing bulk observables but, simultaneously, it is a feature that hampers applicability of the method to, in particular, computation of energy spectra or transition rates. This deficiency can be cured by restoring broken symmetries with the use of projection techniques i.e., by generalizing the SR-DFT to the so-called multireference DFT (MR-DFT). While the former operates with a single reference Slater determinant $|\varphi\rangle$, the latter uses a linear combination of Slater determinants rotated in space (isospace, gauge space) $\hat{R}|\varphi\rangle$ with weights determined by the symmetry group. Furthermore, after mixing states projected from different quasiparticle or particle-hole configurations one is able to reach with these techniques a level of functionality comparable to the nuclear shell-model (NSM).

There are different realizations of DFT-based configuration-interaction methods, see Ref. [2]. The Warsaw group has developed the DFT-NCCI (no-core-configuration-interaction) variant based on the unpaired Skyrme functional

that includes CSB and CIB terms up to next-to-leading (NLO) order and a unique combination of the angular-momentum and isospin projections with an aim to study ISB in $N \approx Z$ nuclei. With this method we were able to compute different observables and pseudo-observables including: isospin impurities [3], ISB corrections to the superallowed $0^+ \to 0^+$ [4] and $T = 1/2$ mirror [5] beta decays as well as mirror- (MDE) and triplet-displacement energies (TDE) [6,7] with the accuracy comparable to the NSM, see Refs. [8–12] and references quoted therein. Recently, we have also applied the DFT-NCCI formalism to compute mirror energy differences (MED) which are defined as follows:

$$MED_J = E^*_{J,T,-T} - E^*_{J,T,T} \tag{1}$$

where E^*_{J,T,T_z} is the excitation energy of a particular state that has a total angular momentum (spin) J, isospin T, and isospin projection T_z. From theoretical perspective MED are very demanding quantities as they are very sensitive to details of the changes in configurations in function of increasing excitation energy and angular momentum. In spite of that we were able to reach reasonable agreement in $T = 1/2$ mirrors from the lower fp shell [13], the $T = 3/2$ ^{47}Ti / ^{47}Mn mirrors [14], and the very heavy $T = 1/2$ ^{79}Zr / ^{79}Y mirrors [15] without adjusting locally a single coupling constant. We failed, however, to reproduce MED for unnatural ($\pi = +$) parity bands in ^{45}Sc / ^{45}Cr. The aim of present work is to investigate sensitivity of DFT-NCCI calculations for MED in $\pi = +$ parity bands in ^{45}Sc / ^{45}Cr with respect to low-energy couplings (LECs) of the local CSB force and with respect to shape degrees of freedom. We report here the first DFT-NCCI calculations for MED that admit not only axial but also triaxial configurations in the model's configuration space. The paper is organized as follows: In Sec. II we briefly introduce the DFT-NCCI model. In Sec. III A we discuss sensitivity of MED in $\pi = +$ parity bands in ^{45}Sc / ^{45}Cr with respect to LECs of the CSB force. In Sec. III B we present the results of calculations that include triaxial configurations. The paper is briefly summarized in Sec. IV

II. THE DENSITY-FUNCTIONAL THEORY NO-CORE-CONFIGURATION-INTERACTION APPROACH

The self-consistent Hartree-Fock(-Bogliubov) framework is a powerful approach offering simple understanding of complex features of nuclear structure in terms of very intuitive deformed independent-particle configurations. It is therefore not surprising that it serves as a starting point for various more advanced theories which, in general, account for interactions between independent-particle configurations provided by a mean field. The DFT-NCCI approaches, see Ref. [2] and references quoted therein for recent overview of different realizations of DFT-NCCI schemes, are good examples of such beyond-mean-field methods. These approaches can be characterized as post Hartree-Fock(-Bogoliubov) configuration-interaction methods that aim to restore symmetries violated by mean-field and mix good symmetry states projected from different mean-field configurations.

We developed recently the DFT-NCCI variant dedicated to study isospin-symmetry-breaking phenomena in $N \approx Z$ nuclei. The model is based upon unpaired charge-dependent local EDF generated by density-independent Skyrme pseudopotential and involves a unique combination of the angular-momentum and isospin projections. In practical calculations we use $\mathrm{SV}^{\mathrm{ISB}}_{\mathrm{T;\,NLO}}$ Skyrme pseudopotential that includes density-independent isoscalar Skyrme pseudopotential SV of Ref. [16] (albeit with tensor terms included in the SV-EDF for the sake of mathematical consistency) augmented with class III CSB interaction:[1]

$$\hat{V}^{\mathrm{III}}(i,j) = \big[t_0^{\mathrm{III}}\delta(\boldsymbol{r}_{ij}) + \tfrac{1}{2}t_1^{\mathrm{III}}[\delta(\boldsymbol{r}_{ij})\boldsymbol{k}^2 + \boldsymbol{k}'^2\delta(\boldsymbol{r}_{ij})] + t_2^{\mathrm{III}}\boldsymbol{k}'\delta(\boldsymbol{r}_{ij})\boldsymbol{k}\big]\big(\hat{\tau}_3^{(i)} + \hat{\tau}_3^{(j)}\big), \tag{2}$$

where $\boldsymbol{r}_{ij} = \boldsymbol{r}_i - \boldsymbol{r}_j$, $\boldsymbol{k} = \frac{1}{2i}(\boldsymbol{\nabla}_i - \boldsymbol{\nabla}_j)$, and $\boldsymbol{k}' = -\frac{1}{2i}(\boldsymbol{\nabla}_i - \boldsymbol{\nabla}_j)$ are the standard relative-momentum operators acting to the right and left, respectively. The three new LECs are equal: $t_0^{\mathrm{III}} = 11 \pm 2$ MeV fm^3, $t_1^{\mathrm{III}} = -14 \pm 4$ MeV fm^5, and $t_2^{\mathrm{III}} = -7.8 \pm 0.8$ MeV fm^5. They have been adjusted globally to all available data on MDEs for $A \geqslant 6$ in Ref. [7], which makes our approach free from adjustable parameters.

The model will be applied to compute MED. As mentioned above, our method allows for rigorous treatment of both rotational and isospin symmetries. We have verified, however, that for the case of positive-parity bands in $A = 45$ mirrors (in the calculation based on axial configurations), the spurious isospin mixing [3] very weakly affects the calculated MED and can be safely omitted. Hence, similar to all other applications of the DFT-NCCI to MED, we shall restrict ourselves to angular-momentum projection only. However, at variance to all other applications of the DFT-NCCI to MED we shall admit, in the final calculations, also triaxial configurations.

For the sake of completeness let us recall the model's computational scheme. It proceeds in three major steps:

(1) First, we compute the so-called a *configuration space*. It consists a set of N_{conf} relevant low-lying (multi)particle-(multi)hole self-consistent Hartree-Fock solutions $\{|\varphi_j\rangle\}_{j=1}^{N_{\mathrm{conf}}}$ which are used in subsequent projection.

(2) Second, we apply the angular-momentum projection to each configuration $\{|\varphi_j\rangle\}$ separately in order to determine the family of states $\hat{P}^I_{MK}|\varphi_j\rangle$ having good angular momentum I and its projection on the intrinsic axis K. Since K is, in general, not conserved we perform also K mixing, which gives us a set of good angular-momentum states $|\varphi_j; IM; T_z\rangle^{(i)}$, which form the so-called *model space*:

$$|\varphi_j; IM; T_z\rangle^{(i)} = \frac{1}{\sqrt{\mathcal{N}^{(i)}_{\varphi_j;IM;T_z}}} \sum_K a_K^{(i)} \hat{P}^I_{MK}|\varphi_j\rangle\,, \tag{3}$$

where K stands for a projection of angular momentum onto the intrinsic z axis while

$$\hat{P}^I_{MK} = \frac{2I+1}{8\pi^2}\int d\Omega D^{I*}_{MK}(\Omega) e^{-i\gamma\hat{J}_z} e^{-i\beta\hat{J}_y} e^{-i\alpha\hat{J}_z} \tag{4}$$

is the standard angular-momentum projection operator.

[1]The class II CIB force is inactive in isospin doublets discussed here and will therefore be omitted

(3) Finally, we perform the mixing of, in general, nonorthogonal states $\{|\varphi_j; IM; T_z\rangle^{(i)}\}$ for all configurations $\{|\varphi_j\rangle\}$ by solving the Hill-Wheeler equation. In effect, we obtain a set of linearly independent DFT-NCCI eigenstates of the form:

$$\left|\psi^{k;IM;T_z}_{\rm NCCI}\right\rangle = \frac{1}{\sqrt{\mathcal{N}^{(k)}_{IM;T_z}}} \sum_{ij} c^{(k)}_{ij} \, |\varphi_j; IM; T_z\rangle^{(i)} , \quad (5)$$

Triaxial configurations imply nonconservation of the intrinsic quantum number K which, in turn, affects accuracy and stability of the calculations. The problem of K mixing is handled in our code by solving, for each spin I and each configuration $|\varphi\rangle \in \{|\varphi_j\rangle\}_{j=1}^{j=n}$ separately, the nonorthogonal Hill-Wheeler (H-W) eigenvalue problem:

$$\sum_{K'} H^I_{KK'} g^{(i)}_{IK'} = E^i_I \sum_{K'} N^I_{KK'} g^{(i)}_{IK'}, \quad (6)$$

where

$$H^I_{KK'} = \langle\varphi|\hat{H}\hat{P}^I_{KK'}|\varphi\rangle, \quad (7)$$

$$N_{KK'} = \langle\varphi|\hat{P}^I_{KK'}|\varphi\rangle, \quad (8)$$

denote the Hamiltonian and norm kernels, respectively. The *model space* is overcomplete. We handle this problem by solving the H-W equation (6) in the *collective basis*, spanned by the *natural states*:

$$|\varphi_j; IM; T_z\rangle^{(m)} = \frac{1}{\sqrt{n_m}} \sum_K \eta^{(m)}_K |\varphi_j; IMK; T_z\rangle. \quad (9)$$

The *natural states* used to construct the *model space* are the eigenstates of the norm matrix:

$$\sum_{K'} N_{KK'} \bar{\eta}^{(m)}_{K'} = n_m \bar{\eta}^{(m)}_K, \quad (10)$$

having eigenvalues $n_m > \zeta$ larger than a certain cutoff parameter ζ. In the present calculation we set $\zeta = 0.01$, which guarantees numerical stability of the method. More details concerning K mixing can be found in Ref. [17].

The states (3) spanning the *model space* are nonorthogonal. The final results are therefore calculated by solving again the H-W equation. At this stage we use the same technique of handling overcomplete bases as outlined above for the case of K mixing, i.e., we compute the eigenvalues and eigenstates of the norm matrix and construct the *natural states* and, in turn, the *collective basis*. In this case we fix the cutoff parameter to be $\chi = 0.01$ in ^{45}Sc and readjust its value in ^{45}Cr in order to obtain the collective basis of the same size in both nuclei.

III. DENSITY-FUNCTIONAL THEORY NO-CORE-CONFIGURATION-INTERACTION RESULTS FOR MIRROR ENERGY DIFFERENCE IN ^{45}Sc / ^{45}Cr-SENSITIVITY STUDY

The DFT-NCCI method used hereafter has been defined in Ref. [18], see also the supplemental material to Ref. [14]. It is the configuration-interaction framework with configuration space which is not fixed like in the conventional NSM but built step-by-step by adding physically relevant low-lying (multi)particle-(multi)hole mean-field configurations until reaching acceptable stability for the calculated observables. Building the configuration space we define first the active Nilsson orbitals $|Nn_z\Lambda\Omega\rangle$, which are relevant for a given problem, and explore low-lying configurations built upon these orbitals. The positive-parity bands discussed here involve particle-hole excitation(s) across the $N = Z = 20$. Hence, the active orbitals in our case include particle-like orbitals $|330\frac{1}{2};\pm i\rangle$, $|321\frac{3}{2};\pm i\rangle$, $|312\frac{5}{2};\pm i\rangle$, and $|303\frac{7}{2};\pm i\rangle$ originating from the spherical $0f_{\frac{7}{2}}$ shell and hole-like orbitals $|211\frac{1}{2};\pm i\rangle$ and $|202\frac{3}{2};\pm i\rangle$ originating from the spherical $0d_{\frac{3}{2}}$ and the $|200\frac{1}{2};\pm i\rangle$ Nilsson orbital originating from the spherical $1s_{\frac{1}{2}}$ subshell. The additional quantum number $r = \pm i$ denotes signature. It reflects the fact that signature symmetry (and parity) were superimposed on our mean-field solutions

All calculations presented below were done using a developing version of the HFODD solver [17,19,20]. In the calculations, we used spherical basis consisting 12 harmonic-oscillator shells. The integration over the Euler angles $\Omega = (\alpha, \beta, \gamma)$ is performed using the Gauss-Chebyshev (over α and γ) and Gauss-Legendre (over β) quadratures with $n_\alpha = n_\beta = n_\gamma = 40$ knots.

The principles of our DFT-NCCI approach were laid down in Ref. [18]. Quantitative applications of the method to compute MED became possible after implementing into the formalism contact CSB terms and adjusting their LECs to MDEs, see Refs. [6,7]. Indeed, it is well known mostly from the earlier NSM studies, see Refs. [12,21,22], that these non-Coulombic sources of ISB are critical both to cure the so-called Nolen-Schiffer anomaly [23] of MDEs as well as in quantitative description of MED versus J [24–28]. The very first calculation of MED with the use of DFT-NCCI approach was communicated by Llewellyn *et al.* [15] who applied the method to the heaviest mirror pair studied so far, the $T_z = \pm\frac{1}{2}$ $A = 79$ mirrors. In Ref. [13] we applied the method to the $T_z = \pm\frac{1}{2}$ mirrors from the lower fp-shell nuclei. In this work the DFT-NCCI results were bench-marked with the shell-model results of Ref. [28]. Recently, we applied the same method to the $T_z = \pm\frac{3}{2}$ mirror pairs in ^{45}Sc / ^{45}Cr and ^{47}Ti / ^{47}Mn. In all these applications we limited ourselves to axial mean-field configurations reaching, in general, reasonable agreement with experimental data with the exception of positive-parity band in ^{45}Sc / ^{45}Cr mirrors where the DFT-NCCI failed to reproduce the overall sign of the MED.

A. Sensitivity to low-energy couplings of the contact charge-symmetry-breaking force

In Ref. [14] we performed a test calculation for the MED in a positive-parity band including the 11 most important axial configurations and three different variants of the model, including (1) the Coulomb interaction alone; (2) the Coulomb plus LO CSB contact force [6]; and (3) the Coulomb plus NLO CSB force [7]. These are reproduced here in Fig. 1 (filled symbols). An unexpectedly strong effect of the NLO CSB force on the calculated MED is apparent, capable, in principle, of overturning its sign. This prompted us to formulate in Ref. [14] a conjecture that the data on MED may offer new

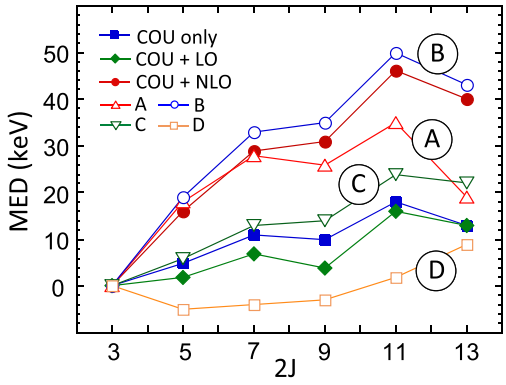

FIG. 1. A test calculation of MED (see text) for the positive-parity states in ^{45}Sc / ^{45}Cr in function of spin $2J$. Full symbols show calculations for three different variants of isospin-breaking force with optimal parameters of the local CSB interaction adjusted to MDEs. The variants include the Coulomb force (blue squares), the Coulomb plus nuclear LO CSB (green diamonds) of Ref. [6], and the Coulomb plus nuclear NLO CSB (red dots) of Ref. [7]. Open symbols show the results of tests performed using A, B, C, and D variants of the NLO CSB force, see the legend and Table I for details concerning parameters of the NLO CSB forces used in the test. In the test calculation we use the same 11 low-lying configurations as in the analogous figure published in Ref. [14].

opportunities to fine tune low-energy coupling constants of the NLO CSB force. Indeed, a fit to MDEs establishes only an overall magnitude of the CSB force without giving an access to its matrix elements which enter the theory through configuration-mixing. Moreover, even the static fit to MDEs is not unique in a sense that the resulting penalty function exhibits quite pronounced softness along the line correlating two out of three LECs [7]:

$$t_1^{\rm III} \approx a\left(t_0^{\rm III} - b\right) - c, \tag{11}$$

where $a = -1.65$ fm^2, $b = 11$ MeV fm^3, and $c = 14$ MeV fm^5. To exploit the conjecture formulated in Ref. [14] we decided to create six variants of the NLO CSB interaction and perform a sensitivity study for MED. The LECs of these new forces are collected in Table I. The variants A and B follow the trend given by Eq. (11) and have the original value of $t_2^{\rm III}$. Note that, in these two cases, the mirror displacement energies (MDE) are very close to the experimental value of 24 MeV. In the variants C and D we fix original values for $t_0^{\rm III}$ and $t_1^{\rm III}$ and vary $t_2^{\rm III}$. In these cases we completely (albeit intentionally) deteriorate the agreement between theoretical and experimental MDEs. The variants E and F have all LECs different than original values. The calculated MDEs are again much worse than for the original force.

TABLE I. Parameters of the NLO CSB forces used to perform sensitivity study of MED with respect to LECs of the effective contact CSB force. Last column shows the calculated values of mirror displacement energy (MDE) defined as binding-energy difference between the $J = 3/2^+$ bandheads of positive-parity bands. Its experimental value is 24 MeV.

NLO Variant	$t_0^{\rm III}$ [MeV fm^3]	$t_1^{\rm III}$ [MeV fm^5]	$t_2^{\rm III}$ [MeV fm^5]	MDE [MeV]
A	−6.0	14.0	−7.8	24.126
B	1.0	2.5	−7.8	24.104
C	11.0	−14.0	0.0	21.705
D	11.0	−14.0	7.8	19.333
E	−6.0	−7.0	0.0	24.667
F	−6.0	−7.0	3.0	23.753

The MED calculated using test forces A, B, C, and D are shown in Fig. 1 (open symbols). The results for the variants E and F appears to be quantitatively similar to the results obtained with the forces C and D, respectively. Hence we refrain from showing them for the sake of clarity. The calculations clearly reveal strong dependence of MED on the gradient-dependent terms. It is rather clear, however, that the NLO force is not capable to change the sign, definitely not without completely deteriorating MDE.

B. Sensitivity to nuclear shape

The configurations included in the configuration-mixing triaxial calculations for ^{45}Sc / ^{45}Cr mirror pair are depicted in Table II. The table has conventional layout introduced in Ref. [15]. Each configuration is represented by a set of symbols encoding occupation numbers. Full dots denote pairwise occupied active Nilsson states while up (down) arrows denote singly occupied active Nilsson states with signature $r = -i$ ($r = +i$), respectively. The figure displays configurations in both members of the mirror pair, with left (right) column of symbols representing each configuration that corresponds to the even (odd) subsystem, respectively. The configurations are grouped, also conventionally, into different types of excitation. We adopt here the scheme worked out in Ref. [14] and divide them into the following groups:

(i) g.s. The first configuration listed in the table represents the global positive-parity ground state.
(ii) Group 1: The simplest p-h seniority-one ($\nu = 1$) excitations obtained by promoting the unpaired nucleon to the empty active orbitals.
(iii) Group 2: Configurations that correspond to $\nu = 1$ nn/pp pairing excitations
(iv) Group 3: These are the lowest seniority-three ($\nu = 3$) configurations having one unpaired nucleon and one broken pair in the even subsystem.
(v) Group 4: These are the lowest seniority-three ($\nu = 3$) configurations having one unpaired nucleon and one broken pair in the odd subsystem.
(vi) Group 5: These are seniority-three ($\nu = 3$) configurations having a hole in sd-shell in an even subsystem.

For the positive-parity $A = 45$ mirrors there are two configurations of Group 1, five of Group 2, eight of Group 3, eight of Group 4, and three of Group 5. The overall number of configurations used here is comparable (only slightly larger) to the set used in Ref. [14]. As before, each configuration, expressed in terms of occupation numbers in Table II, is represented by a single self-consistent Slater determinant. The novel element is that we do not superimpose any constraint on the shape degree

TABLE II. Configurations used in triaxial DFT-NCCI calculations for positive-parity states in ^{45}Sc / ^{45}Cr mirror nuclei. The left (right) column of symbols representing each configuration corresponds to the even (odd) subsystem, respectively, i.e., the table displays mirror-symmetric sets of configurations in both nuclei. Full dots denote pairwise occupied Nilsson states. Up (down) arrows denote singly occupied Nilsson states with signature $r = -i$ ($r = +i$), respectively. Triaxial (axial) configurations are labeled as T (A), respectively.

GROUP	g.s.	1		3						
conf. no.	1	2	3	17	16	4	5	19	20	21
shape	T	A	A	T	T	T	T	A	A	A
$\|303\ 7/2\rangle$										
$\|312\ 5/2\rangle$										
$\|321\ 3/2\rangle$	●	●	●	↑	●	↓	●	↑	●	↓	●	↑	●	↓	●	↑	●
$\|330\ 1/2\rangle$	●	●	●	●	●	↑	●	↑	●	↓	●	↓	●	↑	●	↑	●	↓	●
$\|202\ 3/2\rangle$	↑	●	●	●	●	↑	●	↑	●	↑	●	↑	●	●	●	●	●	●	●
$\|200\ 1/2\rangle$	●	●	↓	●	●	●	●	●	●	●	●	●	●	↓	●	↓	●	↓	●
$\|211\ 1/2\rangle$	●	●	●	●	↓	●	●	●	●	●	●	●	●	●	●	●	●	●	●
GROUP	3	4								5
conf. no.	22	7	6	13	12	23	24	25	26	18
shape	A	T	T	T	T	A	A	A	A	T
$\|303\ 7/2\rangle$										
$\|312\ 5/2\rangle$		↓	↑	↑	↓	↓	↑	↑	↓	↑
$\|321\ 3/2\rangle$	↓	●	↓	↓	↑	↑	↓	↓	↑	↑	●
$\|330\ 1/2\rangle$	↓	●	●	●	●	●	●	●	●	●	●	●	●	●	●	↓	●
$\|202\ 3/2\rangle$	●	●	↑	●	↑	●	↑	●	↑	●	●	●	●	●	●	●	●	↑
$\|200\ 1/2\rangle$	↓	●	●	●	●	●	●	●	●	↑	●	↑	●	↑	●	↑	●	●	●
$\|211\ 1/2\rangle$	●	●	●	●	●	●	●	●	●	●	●	●	●	●	●	●	●	●	●
GROUP	5		2							
conf. no.	14	15	9	8	10	27	28			
shape	T	T	T	T	T	A	A			
$\|303\ 7/2\rangle$										
$\|312\ 5/2\rangle$	↑	↓			●	●		●		
$\|321\ 3/2\rangle$	●	●	●	●			●		●	●
$\|330\ 1/2\rangle$	↑	●	↑	●	●	●	●	●		●
$\|202\ 3/2\rangle$	●	↑	●	↑	↑	●	↑	●	●	●	●
$\|200\ 1/2\rangle$	●	●	●	●	●	●	●	●	↓	●	↓	●
$\|211\ 1/2\rangle$	●	●	●	●	●	●	●	●	●	●	●	●

of freedom which, depending on convergence, can be either triaxial (T) or axial (A), as indicated in the table.

The unconstraint mean-field calculation leads to the g.s. configuration in ^{45}Sc (^{45}Cr) which is slightly triaxial with $\beta_2 \approx 0.29$ and $\gamma \approx 6.8°(6.3°)$, respectively. The triaxial minimum, however, is only 218 keV (^{45}Sc) and 134 keV (^{45}Cr) deeper as compared with the axially deformed g.s. configuration used in Ref. [14]. This indicates pronounced shape softness, at least in the low-spin part of the band. Inclusion of shape vibrations is prohibitively difficult with the present version of our model. Hence, as already discussed, we will represent the g.s. with a single triaxial self-consistent Slater determinant.

The calculation shows that triaxiality has a profound impact on the theoretical MED, in particular inverting their sign. Already by applying the angular-momentum projection to the g.s., without invoking configuration mixing, we obtain acceptably good agreement to data both concerning the sign as well as the magnitude of MED, as shown in Fig. 2. Interestingly this single-configuration-based picture rather weakly changes after admixing excited configurations what is rather atypical. This is visualized in Fig. 3 where we show an impact of specific groups of excitations on MED. Indeed, the admixtures of the excited configurations of Groups 1 and 2 (marked by diamonds) almost do not change the MED obtained with the g.s. configuration alone shown (open triangles) in Fig. 2. The contributions due to the lowest seniority $\nu = 3$ configurations of Groups 3 and 4 tend to cancel each other. Their net effect on MED is small as shown (curve marked by squares) in Fig. 3. The higher excitations of Group 5 do not bring anything new (maybe except of spin $11/2^+$), indicating that our calculations are relatively well converged at low spins. The overall agreement to the data should be considered as satisfactory although we are not able to account for sudden decrease at $J = 11/2^+$.

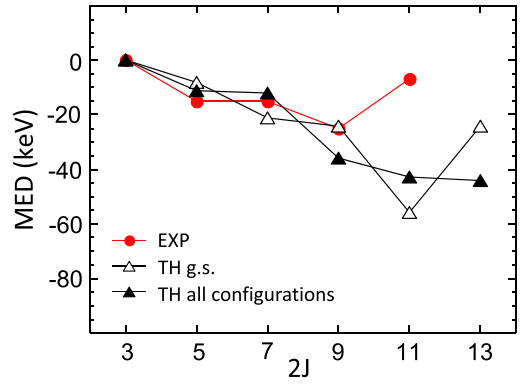

FIG. 2. MED for the positive-parity states in ^{45}Sc / ^{45}Cr as a function of spin $2J$. Experimental data are marked with full (red) dots. Open triangles denote theoretical MED calculated using a single configuration representing g.s. Full (black) triangles represent the result of NCCI calculations involving all configurations listed in Table II.

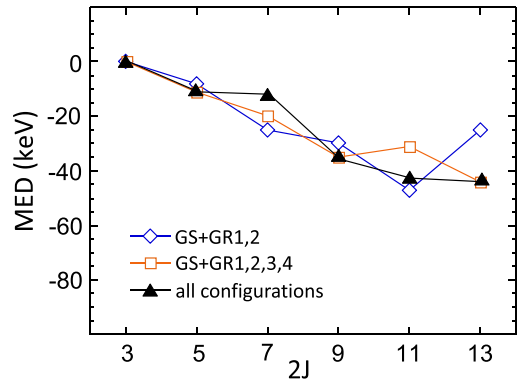

FIG. 3. Theoretical MED for the positive-parity states in ^{45}Sc / ^{45}Cr as a function of spin $2J$. Diamonds (blue) mark theoretical MED calculated using the g.s. and seniority $\nu = 1$ excitations of Groups 1 and 2. Squares (orange) include additionally the lowest $\nu = 3$ excitations of Groups 3 and 4. Full (black) triangles represent the result of NCCI calculations involving all configurations listed in Table II.

Our calculations are in fair overall agreement with the experimental spectra. The calculated excitation energies in the $\pi = +$ parity band in ^{45}Sc are (in MeV): 0.25, 0.60, 1.03, 1.64, 2.19, and 3.06 for $I^\pi = 5/2^+, 7/2^+, 9/2^+, 11/2^+$, and $13/2^+$, respectively. We overestimate the moment of inertia which suggests that pairing entering our theory through configuration mixing is probably too weak and needs to be corrected in future (the quadrupole deformation agrees well with the quadrupole-moment measurement by Avgoulea *et al.* [29]). Shell-model calculations, on the other hand, appear to underestimate the inertia as shown in Ref. [30]. It is interesting to notice that the total Routhian surface (TRS) calculations shown in Ref. [30] indicate that the $\pi = +$ band is slightly triaxial while the $\pi = -$ band is axial, albeit soft, which is in agreement with our calculations.

IV. SUMMARY AND CONCLUSIONS

Low-energy nuclear processes including the superallowed $0^+ \to 0^+$ [9] and $T = 1/2$ mirror [10,11] beta decays allow for precision tests of fundamental symmetries. The tests heavily rely on precision calculations of ISB corrections being a domain of many-body nuclear models. Hence, precision of nuclear tests of the standard model is heavily intertwined with the credibility of nuclear modeling of ISB phenomena.

During the last decade we have been developing a universal theoretical framework based on angular-momentum and isospin projected DFT to study ISB-related phenomena in $N \approx Z$ nuclei. The rationale behind choosing DFT-based method is their natural ability to account in a self-consistent way both the short- and long-range physics associated with strong and electromagnetic forces, respectively. The model appeared to be very successful in reproducing and predicting diverse observables and pseudo-observables associated with ISB effects from elusive isospin impurities [3] to mirror energy differences (MED) [13,15] in rotational bands versus angular momentum with the only exception of MED in the positive-parity mirror bands in ^{45}Sc / ^{45}Cr [14]. In this case we failed to reproduce an overall sign of the MED what casts a shadow on an overall good performance of our model and undermines its credibility.

In this work we performed a thorough analysis of the MED in $\pi = +$ bands of ^{45}Sc / ^{45}Cr mirror pair, focusing on two aspects: (*i*) sensitivity with respect to parameters of the effective contact CSB force and (*ii*) sensitivity with respect to nuclear shape. We have demonstrated that even large variations of the parameters of the contact CSB NLO force cannot invert sign of the calculated MED, at least not without deteriorating MDE for the $J = 3/2^+$ bandheads. Our calculations reveal, on the other hand, strong dependence of the calculated MED on the shape of $\pi = +$ ground-state configuration. The unconstraint Hartree-Fock solution for the $\pi = +$ g.s. configuration is triaxial and corresponds to $\beta_2 \approx 0.29$ and $\gamma \approx 6.8^\circ(6.3^\circ)$ in ^{45}Sc (^{45}Cr), respectively. Inclusion of triaxial $\pi = +$ g.s. configuration in the DFT calculations not only inverts the sign of the calculated MED but also reproduces a magnitude of the MED without any need for further adjustment of the model's LECs. These two conclusions essentially do not depend on configuration mixing which weakly affects the calculated MED. The physical mechanism staying behind such a radical change in dynamics of ISB effects along the rotational path is not clear and requires further studies.

ACKNOWLEDGMENT

This work was supported by the Polish National Science Centre (NCN) under Contract No. 2018/31/B/ST2/02220.

[1] E. M. Henley and G. A. Miller, *Mesons in Nuclei*, edited by M. Rho and D. H. Wilkinson (North Holland, Amsterdam, 1979).
[2] J. A. Sheikh, J. Dobaczewski, P. Ring, L. M. Robledo, and C. Yannouleas, J. Phys. G **48**, 123001 (2021).
[3] W. Satuła, J. Dobaczewski, W. Nazarewicz, and M. Rafalski, Phys. Rev. Lett. **103**, 012502 (2009).
[4] W. Satuła, J. Dobaczewski, W. Nazarewicz, and M. Rafalski, Phys. Rev. Lett. **106**, 132502 (2011).
[5] M. Konieczka, P. Bączyk, and W. Satuła, Phys. Rev. C **105**, 065505 (2022).
[6] P. Bączyk, J. Dobaczewski, M. Konieczka, W. Satuła, T. Nakatsukasa, and K. Sato, Phys. Lett. B **778**, 178 (2018).
[7] P. Bączyk, W. Satuła, J. Dobaczewski, and M. Konieczka, J. Phys. G **46**, 03LT01 (2019).
[8] J. C. Hardy and I. S. Towner, Phys. Rev. C **91**, 025501 (2015).
[9] J. C. Hardy and I. S. Towner, Phys. Rev. C **102**, 045501 (2020).
[10] O. Naviliat-Cuncic and N. Severijns, Phys. Rev. Lett. **102**, 142302 (2009).
[11] M. Gonzalez-Alonso, O. Naviliat-Cuncic, and N. Severijns, Prog. Part. Nucl. Phys. **104**, 165 (2019).
[12] W. Ormand and B. Brown, Nucl. Phys. A **491**, 1 (1989).
[13] P. Bączyk and W. Satuła, Phys. Rev. C **103**, 054320 (2021).
[14] S. Uthayakumaar, M. A. Bentley, E. C. Simpson, T. Haylett, R. Yajzey, S. M. Lenzi, W. Satuła, D. Bazin, J. Belarge, P. C. Bender, P. Davies, B. Elman, A. Gade, H. Iwasaki, D. Kahl, N. Kobayashi, B. Longfellow, S. J. Lonsdale, E. Lunderberg, L. Morris, D. R. Napoli, T. Parry, X. Pereira-Lopez, F. Recchia, J. A. Tostevin, R. Wadsworth, and D. Weisshaar, Phys. Rev. C **106**, 024327 (2022).
[15] R. D. O. Llewellyn, M. A. Bentley, R. Wadsworth, J. Dobaczewski, W. Satuła, H. Iwasaki, G. de Angelis, J. Ash, D. Bazin, P. C. Bender, B. Cederwall, B. P. Crider, M. Doncel, R. Elder, B. Elman, A. Gade, M. Grinder, T. Haylett, D. G. Jenkins, I. Y. Lee, B. Longfellow, E. Lunderberg, T. Mijatović, S. A. Milne, D. Rhodes, and D. Weisshaar, Phys. Lett. B **811**, 135873 (2020).
[16] M. Beiner, H. Flocard, N. Van Giai, and P. Quentin, Nucl. Phys. A **238**, 29 (1975).
[17] J. Dobaczewski, W. Satuła, B. Carlsson, J. Engel, P. Olbratowski, P. Powałowski, M. Sadziak, J. Sarich, N. Schunck, A. Staszczak, M. Stoitsov, M. Zalewski, and H. Zduńczuk, Comput. Phys. Commun. **180**, 2361 (2009).
[18] W. Satuła, P. Bączyk, J. Dobaczewski, and M. Konieczka, Phys. Rev. C **94**, 024306 (2016).

[19] N. Schunck, J. Dobaczewski, W. Satuła, P. Bączyk, J. Dudek, Y. Gao, M. Konieczka, K. Sato, Y. Shi, X. Wang, and T. Werner, Comput. Phys. Commun. **216**, 145 (2017).
[20] J. Dobaczewski, P. Bączyk, P. Becker, M. Bender, K. Bennaceur, J. Bonnard, Y. Gao, A. Idini, M. Konieczka, M. Korteleinen, L. Próchniak, A. Romero, W. Satuła, Y. Shi, T. Werner, and L. Yu, J. Phys. G **48**, 102001 (2021).
[21] G. Colò, H. Sagawa, N. Van Giai, P. F. Bortignon, and T. Suzuki, Phys. Rev. C **57**, 3049 (1998).
[22] B. A. Brown, Phys. Rev. Lett. **85**, 5296 (2000).
[23] J. A. Nolen, Jr and J. P. Schiffer, Annu. Rev. Nucl. Sci. **19**, 471 (1969).
[24] A. P. Zucker, S. M. Lenzi, G. Martínez-Pinedo, and A. Poves, Phys. Rev. Lett. **89**, 142502 (2002).
[25] M. Bentley and S. Lenzi, Prog. Part. Nucl. Phys. **59**, 497 (2007).
[26] K. Kaneko, Y. Sun, T. Mizusaki, and S. Tazaki, Phys. Rev. Lett. **110**, 172505 (2013).
[27] K. Kaneko, Y. Sun, T. Mizusaki, and S. Tazaki, Phys. Rev. C **89**, 031302(R) (2014).
[28] M. A. Bentley, S. M. Lenzi, S. A. Simpson, and C. A. Diget, Phys. Rev. C **92**, 024310 (2015).
[29] M. Avgoulea *et al.*, J. Phys. G **38**, 025104 (2011).
[30] P. Bednarczyk *et al.*, Phys. Lett. B **393**, 285 (1997).